JOURNAL OF SPACECRAFT AND ROCKETS
Vol. 32, No. 6, November–December 1995

Aerodynamics of a Body Immersed in a Supersonic Wake: A Computational Study

Curtis C. Ober* and J. Parker Lamb†
University of Texas at Austin, Austin, Texas 78712
and
Thomas M. Kiehne‡
Institute for Advanced Technology, Austin, Texas 78759

The objective of this investigation was to determine the aerodynamic characteristics of a trailing body in a supersonic wake. The effects of two leading-body geometries and various axial and radial placements of the trailing body were examined. At locations downstream of the wake neck and coaxial with the leading body, a toroidal vortex was formed at the nose of the trailing body. When the trailing body was displaced radially, the toroidal vortex was replaced with a horseshoe vortex, which diminished in size with increasing displacement. For the coaxial alignments, the drag on the trailing body was substantially reduced below its freestream value, but increased with increasing separation distance. For off-axis alignments, the drag also increased with exposure to freestream conditions. The variation of lift coefficient with asymmetry indicated that the trailing body would tend to move towards the wake centerline, but the pitching moment suggested that an angle of attack would develop and could cause the trailing body to be ejected from the wake core.

Nomenclature

C_D	= drag coefficient, $D_f/[(1/2)\rho_\infty U_\infty^2((1/4)\pi D^2)]$
C_L	= lift coefficient, $L_f/[(1/2)\rho_\infty U_\infty^2((1/4)\pi D^2)]$
C_M	= moment coefficient, $M/[(1/2)\rho_\infty U_\infty^2((1/4)\pi D^3)]$
D	= base diameter of body
d_{so}	= shock standoff distance (trailing body)
$\boldsymbol{F}, \boldsymbol{G}, \boldsymbol{H}$	= flux vectors
L	= length of body
L_C	= characteristic body length
M	= pitching moment about x_{cm}, (CW +)
Ma	= Mach number
Ma_{so}	= Mach number upstream of shock at centerline
P	= penetration depth
p	= static pressure
p_0	= freestream stagnation pressure
p_∞	= freestream static pressure
$\boldsymbol{Q}$	= solution vector
Re_a	= Reynolds number based on the speed of sound
r	= radial coordinate
$\boldsymbol{S}$	= stress vector
T_0	= stagnation temperature
U_∞	= freestream velocity
x	= axial coordinate
$x_{c.m.}$	= center of mass measured from nose
$x_{c.p.}$	= center of pressure measured from nose
Δ	= an incremental difference
$\Delta X_{c.p.}$	= static margin
ξ, η, ζ	= generalized coordinates
τ	= generalized time

Introduction

IN the development of antiarmor projectiles, an important parameter is the penetration depth, which is a measure of projectile effectiveness. Contemporary projectile designs depend on high kinetic energy, rather than an explosive charge, for penetration. Speeds are routinely in the supersonic regime and can approach hypersonic conditions. The conventional projectile configuration is simply a long rod penetrator. However, recent studies[1,2] have shown that enhanced penetration is possible if the long rod is segmented into multiple bodies.

As is shown in Fig. 1, enhanced penetration is not always achieved. Suggested reasons for the variation of P/L_C include (for $\Delta x/D < 2$) that segment $i+1$ reaches the crater bottom before segment i has completed its penetration,[1] (for $\Delta x/D > 2$) that backflowing material disturbs incoming segments,[1] and the misalignment of segments.[2] The first two possibilities are in the area of penetration mechanics, but the last relates to multiple-body aerodynamics, and is the primary motivation for this research. The trailing segments will have an alignment that is dependent on their wakes and aerodynamic characteristics. Thus, the flight trajectory of multiple segments is of critical importance in obtaining enhanced penetration by segmented projectiles.

Experimental studies of multibody configurations, with one body in the supersonic wake of another, are very limited. However, some information is obtainable from investigations[3,4] carried out during the 1960s. These studies examined flow past an axisymmetric backward-facing step and a missile–nozzle configuration. The primary information gained from these studies is that the surface pressure of the trailing body follows the same trends as the centerline static pressure behind a single body. For example, along the centerline the static pressure near the base plane is below freestream pressure, and increases as one moves towards the region of shear-layer reattachment. The static pressure peaks after reattachment and decays slowly to freestream conditions further downstream. These trends in pressure are also consistent with two-dimensional reattaching shear layers. More recently, Berner[5] investigated experimentally various cone–cylinder geometries behind a cylinder. Reported information included surface pressures on both the leading and trailing bodies, and LDV measurements within the flowfield.

Berner[5] also included computational results related to his experiments. The results were in fair agreement and showed the most difficult region of the flowfield to predict is the recirculation zone between the tandem bodies. This conclusion is consistent with computations of single-body flowfields. The only other computation known by the author related to these multibody configurations is that of Sahu and Nietubicz.[6] Their investigation revealed a large drag reduction for trailing bodies.

Presented as Paper 94-3519 at the AIAA Atmospheric Flight Mechanics Conference, Scottsdale, AZ, Aug. 1–3, 1994; received Aug. 31, 1994; revision received March 1, 1995; accepted for publication March 7, 1995.

*Graduate Research Assistant, Department of Mechanical Engineering; currently Limited Term Ph.D. Appointee, Sandia National Laboratories, Org. 1421, MS 1111, Albuquerque, NM 87185-1111. Member AIAA.
†Ernest Cockrell Jr. Memorial Professor, Department of Mechanical Engineering. Associate Fellow AIAA.
‡Director, Hypervelocity Physics. Senior Member AIAA.

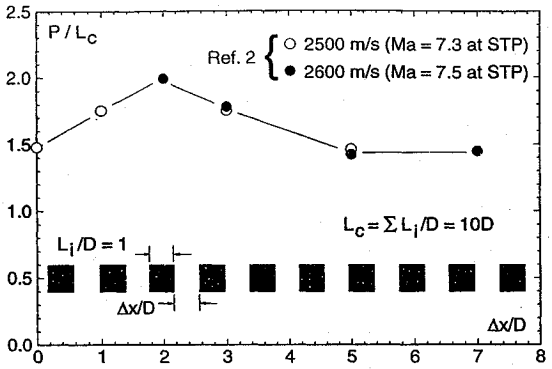

Fig. 1 Penetration depth for various separation distances.

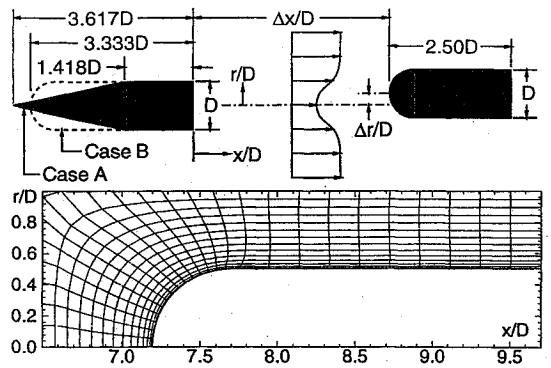

Fig. 2 Schematic of tandem body flowfield and representative grid around trailing body.

In our investigation, a simple tandem-body configuration was used to examine the basic aerodynamic trends of segmented penetrators, and the results presented here are some of those more extensively discussed in Ref. 7. To achieve this objective, numerical simulations of the flowfield generated by two leading-body geometries and the trailing body at various axial and radial placements were computed. Figure 2 shows geometric parameters for the tandem bodies, and the freestream conditions were set to $Ma = 4.95$, $Re_D = 1.25 \times 10^6$, $U_\infty = 765$ m/s, $T_0 = 353$ K, and $p_0 = 2080$ kPa. Unlike an earlier investigation,[6] the leading and trailing bodies are of the same diameter. The trailing body was designed to be blunt in order to more closely match the flat-faced cylinders of Fig. 1. The hemispherical nose allowed easier grid generation because of the elimination of sharp corners. However, this nose geometry differs from that of Berner,[5] who considered cone–cylinder bodies in a supersonic wake.

The two leading-body configurations considered herein were a 12-deg cone–cylinder (case A) and a hemisphere–cylinder (case B), which produced significantly different wakes and allowed the effects of different velocity profiles to be assessed. Various axial separations ($\Delta x/D = 1.88, 4.63, 7.20$ for cases A and B with $\Delta r/D = 0.0$) and radial displacements ($\Delta r/D = 0.0, 0.05, 0.15, 0.25$ for case A with $\Delta x/D = 7.20$) were also examined to study the effects of wake development and offset on the trailing-body aerodynamics. The forces and moments on the trailing body are of primary concern, so that it may be ascertained whether the trailing body will remain in the wake or be ejected from it. It is believed that the present results lead to an improved understanding of the aerodynamics of segmented projectiles, which affects the flight dynamics of the segmented array.

Computational Technique

The system of equations used in this investigation was the thin-layer, Reynolds-averaged Navier–Stokes equations.[8] In generalized coordinates, they can be written as

$$\partial_\tau \boldsymbol{Q} + \partial_\xi \boldsymbol{F} + \partial_\eta \boldsymbol{G} + \partial_\zeta \boldsymbol{H} = Re_a^{-1} \partial_\zeta \boldsymbol{S} \qquad (1)$$

The solution algorithm is an implicit finite-difference scheme[8] with flux-vector splitting in the streamwise direction and central differencing in the other directions.[9] Although the mean flow is steady (i.e., neither the separation distance $\Delta x/D$ nor the displacement distance $\Delta r/D$ varies with time), the solutions were obtained in a time-asymptotic fashion. The grid scheme was a zonal method that separates the flowfield into smaller components. Communication between the zones ensured the solution was continuous across zone boundaries.[10,11]

In Fig. 2, a representative grid around the trailing body is shown for every fourth grid line, where a typical grid contained 101×61 points. To handle the transverse curvature associated with the axisymmetric geometry, three planes were used in the circumferential direction with a separation angle of 5 deg. For cases with radial displacement, an axisymmetric flowfield no longer existed, and a half-plane solution (180 deg) was required. Therefore 19 planes with a separation angle of 11.25 deg, were used for the half-plane solution. The two additional planes, for a total included angle of 202.5 deg were required to enforce boundary conditions across the symmetry plane. The applied boundary conditions were as follows for axisymmetric cases: symmetry across the centerline ($r/D = 0.0$), nonreflecting condition at the outermost radial boundary, adiabatic and no-slip conditions at the wall, user-defined wake profiles along the inflow boundary for $\Delta x/D = 4.63$ and 7.20 cases, and extrapolation along the outflow boundary. For off-axis cases, the boundary conditions were the same except along the trailing-body centerline, where averaging of neighbor quantities was used to specify values along the centerline.

A modified form of the Baldwin–Lomax (BL) turbulence model[12] was used in the present study. For example, the intermittency factor was adjusted to allow for the free shear layer being located off the wake centerline behind the leading body.[13] Also, the velocity difference across the shear layer was corrected to allow negative minimum velocities.[14] Within the wake, the inner region of eddy viscosity was neglected, since the no-slip condition along the centerline is not applicable. Finally, the BL model was applied along the wake (i.e., lines normal to the centerline) and along the trailing body (i.e., lines normal to the body) for coaxial alignments, see Fig. 2. To determine which value of the turbulent viscosity should be used, a simple proximity rule was developed. If the point of interest was nearer the centerline, the turbulent viscosity calculated from the wake was used; otherwise, the turbulent viscosity was determined from the boundary layer.[7]

The thin-layer approximation and the BL model were tested to verify their application to the large recirculation zone behind a single body.[7] For small regions of separation, thin-layer solutions have been found by several other investigators to be equivalent to full Navier–Stokes solutions.[15] Within a large recirculation zone, the thin-layer approximation and the BL model were expected to perform poorly in comparison with experimental data.[9] However, downstream of reattachment ($x/D > 1.5$), comparisons between the computational and experimental results suggested the thin-layer approximation and the BL model were adequate, as can be seen in Figs. 3 and 4. In Fig. 3, experimental data[16] are shown in comparison with predictions of the BL model and the $k-\epsilon$ model.[9] It is observed that the BL model performed as well as the $k-\epsilon$ model after reattachment. Comparisons of predicted and measured[17] pitot pressures at x/D between 2 and 5 are shown in Fig. 4 and exhibit generally good agreement, except for predicting the trailing shock at a slightly larger radial location. Thus, although the computational method was inadequate within the recirculation zone, it is considered satisfactory for the near wake and thus can supply upstream conditions for the trailing body at $\Delta x/D = 4.63$ and 7.20.

For cases with $\Delta x/D = 1.88$, it was found that the shear layer bridged the two bodies and formed a highly modified recirculation zone. Thus, unlike the larger separation distances, where the flow around the leading body can be decoupled from the flow around the trailing body (because of supersonic flow between them), the small separation ($\Delta x/D = 1.88$) caused a coupling between the bodies and required a single computation for the entire region. Because of poor predictions within the recirculation zone, computational results of the flowfield with $\Delta x/D = 1.88$ should be viewed as

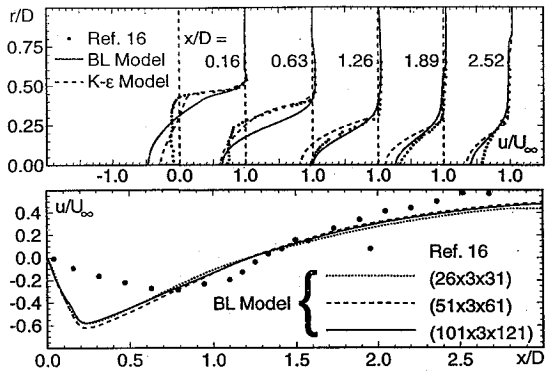

Fig. 3 Parameters in the wake of a single body. Top: streamwise velocity profiles at various axial positions. Bottom: variation of centerline velocity in the wake for three grid resolutions.

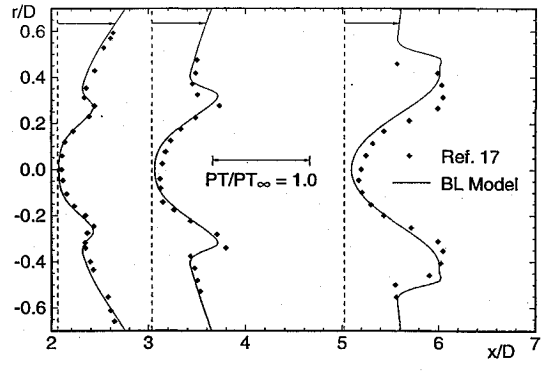

Fig. 4 Pitot-tube pressure profiles at various axial positions behind a 5.9-deg-half-angle cone.

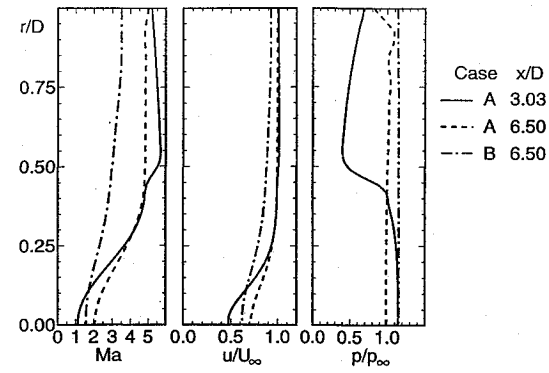

Fig. 5 Computed wake profiles approaching trailing body.

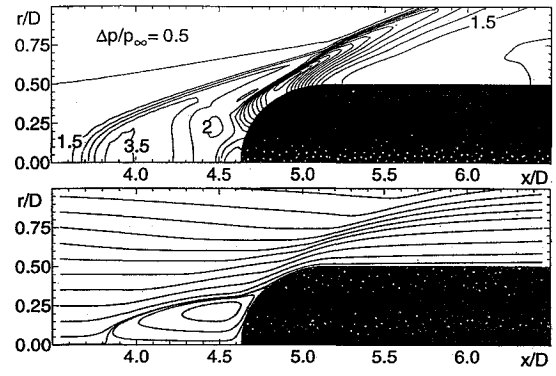

Fig. 6 Pressure contours and streamlines for case A with $\Delta x/D = 4.63$.

approximate, although the corresponding aerodynamic results are included in later sections. Additionally, a grid independence study was completed for the single-body wake[16] and the results are shown in Fig. 3. As can be seen, the centerline streamwise velocity, a key wake flow parameter, is largely independent of the mesh size; however, Fig. 3 illustrates clearly the inadequacies of the thin-layer approximation and the BL model within the recirculation zone.

Flowfield Results for Axisymmetric Cases

The wake profiles of Fig. 5 were determined from leading-body calculations and included the turbulent recirculation region and wake using the BL model as described earlier. The profile for case A at $x/D = 3.03$ indicates a Mach-number variation of $Ma \approx 1$ to 5 over $r/D \approx 0$ to 0.5, while at $x/D = 6.50$, the Mach number varies from $Ma \approx 2$ to 5 over $r/D \approx 0$ to 0.5. In contrast, the profile for case B at $x/D = 6.50$ varies from $Ma \approx 1.5$ to 3 over $r/D \approx 0$ to 0.5. These wake profiles provided the inflow conditions for the trailing-body computations at $\Delta x/D = 4.63$ and 7.20.

In Fig. 6, the pressure contours and streamlines are shown for case A with $\Delta x/D = 4.63$. It is seen that two shocks are formed upstream of the trailing body. One begins at $x/D \approx 3.7$ and intercepts the second shock, which originates above the reattachment point. This behavior can be explained by the streamlines presented in Fig. 6. The first shock wave is caused by a toroidal vortex at the nose of the trailing body, and the origin of this recirculating fluid is the high pressure at the shoulder of the trailing body. For example, the Mach number approaching along $r/D \approx 0.5$ is approximately 5. Thus, nearly freestream conditions are impinging on the shoulder, creating a high-pressure region, which interacts with the low-momentum fluid along the centerline and causes the flow to separate and recirculate.

This recirculating flow is very similar to that experimentally investigated for hypersonic flow past spiked cones.[18] The spike has associated with it a momentum deficit (i.e., the boundary layer); thus at the shoulder, the impinging flow causes a high pressure, which impedes the low-momentum flow along the spike and creates a toroidal vortex. In our case of the blunt trailing body submerged within the wake, the reattachment pressure will interact with the wake momentum deficit and produce a flow pattern similar to the type-D flow,[18] which has an unsteady recirculation region. For type-D flow, Wood[18] states, "For angles slightly greater than the conical detachment angle, the oscillation appears as a ripple in the flow pattern instead of the violent expansion and collapse of the [recirculation] region, which occurs on really blunt bodies." Thus, the flowfield around the blunt body will likely be unsteady in nature, but it is thought that the predicted mean flow variables will be largely unaffected.

In Fig. 7, the pressure contours and streamlines around the trailing body are shown for case A with $\Delta x/D = 7.20$. Unlike the shock formation of case A with $\Delta x/D = 4.63$, only one shock wave is present, but it has a "wiggle" in its shape due to the toroidal vortex field, which exhibits a low-pressure region near its center. The flow stagnation point along the centerline is at $x/D = 6.91$, and the centerline static pressure at $x/D = 6.95$ ($p/p_\infty = 6.23$) is within 1% of the stagnation pressure behind a normal shock for the centerline conditions upstream of the shock wave. Thus the pressure within the vortex correlates closely with the stagnation pressure behind a normal shock. The shock standoff distance, d_{so}/D, is approximately 0.37, while the peak surface pressure occurs just downstream of reattachment and has a value of $p/p_\infty = 10.3$. It is observed that the streamlines in Fig. 7 have a similar pattern to those in Fig. 6.

For case B with $\Delta x/D = 7.20$, the incoming wake was specified along $x/D = 6.50$ using wake profiles shown in Fig 5. Although the centerline Mach number is 1.6, the Mach number at $r/D = 0.5$ is only 3 because the momentum deficit produced by the blunt leading body is spread over a much larger area than for the sharp leading body (case A). The corresponding pressure contours in Fig. 8 show a single bow shock in front of the trailing body. The shock standoff distance is $0.32D$, and the recirculation zone is somewhat smaller than in case A, with $\Delta x/D = 7.20$. It has been assumed that the steady-state toroidal vortices computed here would exist and that turbulent fluctuations of the incoming wake perturb their structure. However, it is possible that these toroidal structures are unsteady in nature and have periods of expansion and collapse.[18]

Inasmuch as the accuracy of inflow-wake profiles (predicted by the present model) was of concern, a series of computations were made using perturbed profiles. Details of this phase of the study are

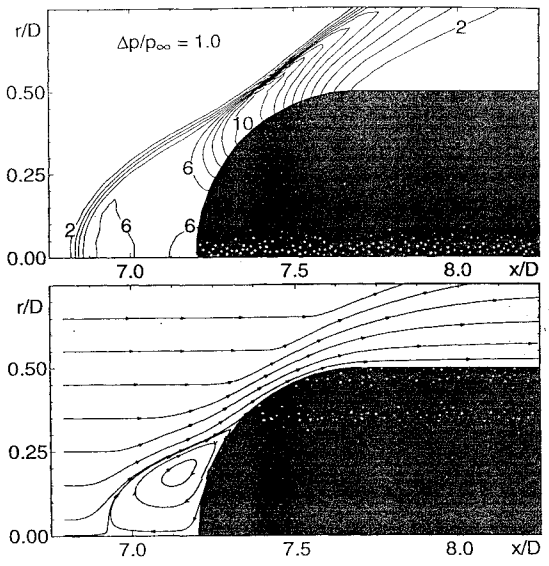

Fig. 7 Pressure contours and streamlines for case A with $\Delta x/D = 7.20$.

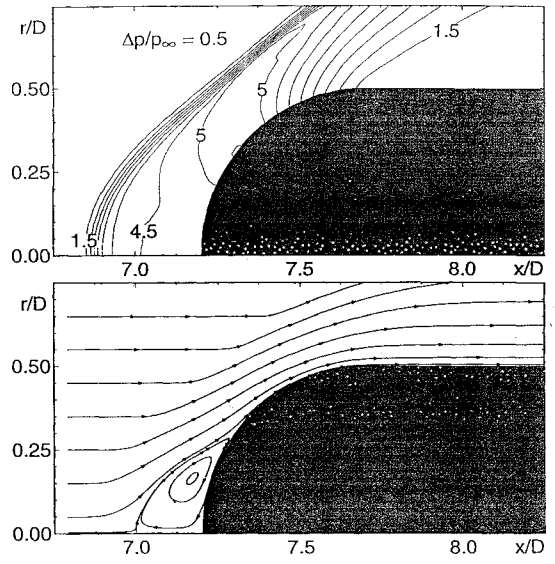

Fig. 8 Pressure contours and streamlines for case B with $\Delta x/D = 7.20$.

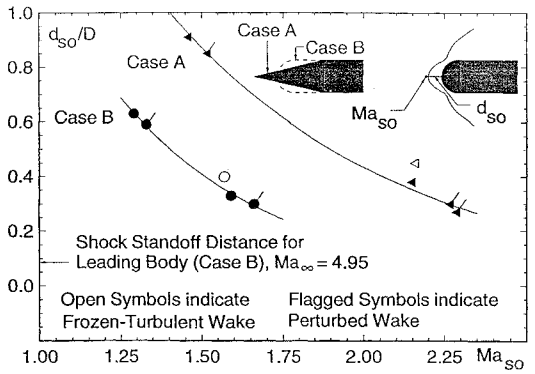

Fig. 9 Shock-wave standoff distance for various centerline Mach numbers upstream of shock wave.

given elsewhere,[7] but the results can be summarized as follows, and Fig. 9 illustrates some of these results. Perturbations that increased the static pressure at the reattachment location tended to increase the size of the toroidal vortex (thus causing the centerline flow to separate farther upstream), whereas perturbations that increased the centerline Mach number tended to decrease the size of the toroidal vortex (i.e., the pressure within the vortex was determined by the centerline stagnation pressure behind the shock). Thus a "critical" separation distance should be expected at some large axial distance, where the momentum of the fluid along the centerline is sufficient to completely overcome the reattachment pressure. At this location, the toroidal vortex would be replaced by a regular stagnation flow at the nose.

Flowfield Results for Off-Axis Cases

For the off-axis simulations, a vertical plane of symmetry was used to reduce the computational domain by nearly one half. The incoming wake of the sharp, leading body (case A) was specified on the grid boundary along $x/D = 6.50$. Because of the complexity of the flowfield, the turbulent wake between $x/D = 6.50$ and the trailing body could not be calculated easily. The BL algebraic turbulence model requires a baseline position from which to measure the moment of vorticity. With the trailing body offset from the wake centerline, a proper normal direction was difficult to formulate. Therefore, the wake turbulence was neglected for the radially displaced cases only, but the turbulent flow within the trailing-body boundary layer was calculated with the BL model (i.e., frozen turbulent wake). From Fig. 9, it can be seen that neglecting the turbulent viscosity between $x/D = 6.5$ and the trailing-body nose for coaxial alignments changes the shock standoff only slightly at the large separation distances. Further discussion of the effects of inflow boundary conditions is given elsewhere.[7,19]

Figure 10 illustrates streamlines in the plane of symmetry for $\Delta r/D = 0.05$. The flow impinging near the nose is recirculated in a vortex structure that is no longer toroidal. The streamline that approaches along $r/D = 0.15$ is deflected toward the stagnation point on the upper part of the body, but then turns downward across the nose and becomes nearly coincident with the streamline that approaches along $r/D = -0.15$. Thus, the fluid between these two streamlines must pass around the sides of the trailing body. This suggests a structure similar to a horseshoe vortex.[20]

Also seen in Fig. 10 are the pressure contours around the trailing body, which indicate that the bow shock bulges into the low-momentum wake core. An unusual feature of this flow is the off-body stagnation point just below the body nose, which has a pressure ratio of 6, as compared to a value of 4 at the center of the horseshoe vortex. The maximum shock standoff distance is $0.4D$, which is slightly larger than in the coaxial case A with $\Delta x/D = 7.20$, where the shock standoff distance was $0.37D$. This increase in shock standoff is likely due to the lack of turbulence computed within the wake. The maximum pressure ratio on the body surface is 15.5, which is roughly half the stagnation pressure under freestream conditions.

Although not shown, results for case A with $\Delta x/D = 7.20$ and $\Delta r/D = 0.15$ indicated that the horseshoe vortex had diminished in size, and the upper reattachment point had shifted down towards the trailing-body nose.[7] In Fig. 11, the streamlines are shown for case A with $\Delta x/D = 7.20$ and $\Delta r/D = 0.25$. The streamlines originating near $r/D \approx 0$ again coalesce as they proceed downstream, again suggesting that the fluid between these streamlines leaves the plane of symmetry and passes around the sides of the trailing body. For this case, the stagnation point moved closer to the trailing-body nose, but neither a nose vortex nor any off-body stagnation points were found.

Referring to the pressure contours of Fig. 11, it is observed that the concave portion of the shock wave has almost disappeared and the bulge at the wake core is less pronounced than for smaller offset cases. The shock standoff distance is $0.2D$ at the centerline, whereas at $r/D = 0.25$ it is approximately $0.1D$, which is nearly the same as that for the blunt body ($0.083D$) in uniform freestream conditions. The maximum surface pressure ratio was determined to be $p/p_\infty = 25.5$. Each of these comparisons supports the notion that further increases of the displacement $\Delta r/D$ will produce surface conditions (upper half of body) that are nearly equivalent to the blunt body in uniform freestream conditions.

In Fig. 12, the surface streamlines (defined by the velocity-vector direction as one approaches the wall[20] and determined by the first grid point away from the body surface) are shown for case A with $\Delta x/D = 7.20$ and $\Delta r/D = 0.05$. The points labeled A mark a high-pressure ring that is associated with stagnation. On the upper half of the nose, the stagnation pressure is high; the pressure on the

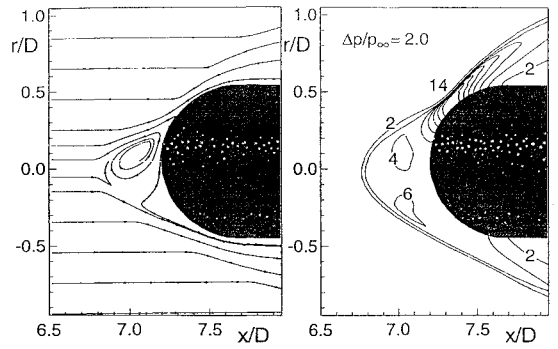

Fig. 10 Streamlines and pressure contours for case A with $\Delta x/D$ = 7.20 and $\Delta r/D$ = 0.25.

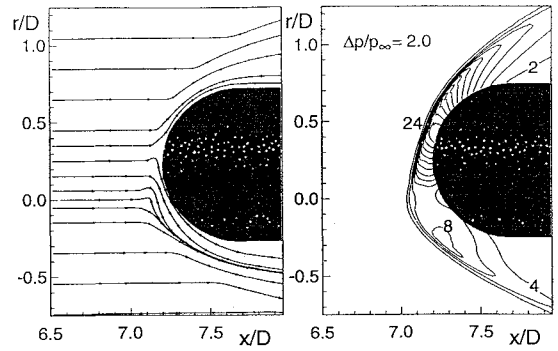

Fig. 11 Streamlines and pressure contours for case A with $\Delta x/D$ = 7.20 and $\Delta r/D$ = 0.25.

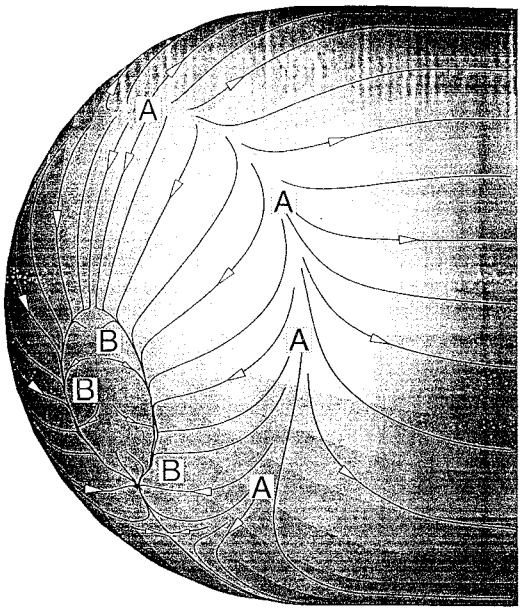

Fig. 12 Surface streamlines around the trailing body, case A, with $\Delta x/D$ = 7.20 and $\Delta r/D$ = 0.05. The labels *A* mark the high-pressure ring and *B* the separation ring.

lower half is substantially smaller. Within the high-pressure ring, all streamlines proceed towards the separation ring, labeled *B*. Some of the streamlines originate on the upper half of the body and continue to the lower half of the body as they proceed downstream.

Aerodynamic Results for Axisymmetric Cases

Drag forces were determined by integrating the pressure and skin friction over the entire surface. The base pressure was assumed constant[7,16] on the trailing body only, and its base drag was found using a recent correlation.[21] This reduced the computational costs by eliminating the recirculation zone behind the trailing body. Drag

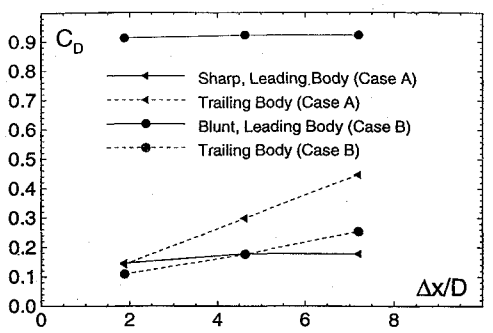

Fig. 13 Drag coefficients for tandem bodies (cases A and B) at different separation distances $\Delta x/D$.

coefficients for the leading and trailing bodies are shown in Fig. 13. In case A, the drag coefficients for leading and trailing bodies are of the same relative magnitude. At $\Delta x/D = 1.88$, the drag coefficients for the leading and trailing bodies are nearly equal, suggesting that the tandem bodies will keep their relative separation. As the separation distance is increased, the drag coefficient on the leading body increases to its freestream value of 0.178 (i.e., the value that would exist if the trailing body were absent). At the short separation distance, the presence of the trailing body increases the pressure on the leading-body base plane, thus reducing the leading-body drag. Berner[5] found similar trends on the base drag of the leading body when the separation distance was small. The drag coefficient on the trailing body increases almost linearly with separation distance for the range computed, approaching slowly its freestream value of approximately 0.92. This value of drag coefficient would not be realized for many base diameters, because the effect of the far wake will persist.

In case B with $\Delta x/D = 1.88$, the drag coefficient on the leading body is reduced slightly by the presence of the trailing body. When the trailing body is moved downstream, the drag coefficient for the leading body tends toward its freestream value (0.92). The drag coefficient for the leading body (case B) is much larger than that associated with the trailing body, and one would expect the two bodies to converge. Once again the drag coefficient on the trailing body increases with separation distance, but at a lower rate than in case A. This is due to the broader wake generated by the blunt leading body, which produces a lower than freestream Mach number impinging on the trailing body. One would expect the drag coefficient for the trailing body in case B to approach its freestream value much farther downstream than that for the trailing body in case A.

Aerodynamic Results for Off-Axis Cases

For the off-axis flow simulations described earlier, it was possible to compute not only the drag coefficients but also lift and pitching-moment coefficients. In determining the base-drag coefficient for the trailing body from the correlation,[21] the effects of varying shoulder Mach number and pressure around the cylinder base were neglected. Moments were calculated about the center of mass, with a positive moment being clockwise. The variations of force and moment coefficients with radial displacement are presented in Fig. 14. As expected, the drag coefficient increases as the trailing body becomes more exposed to freestream conditions (i.e., increasing $\Delta r/D$). The lift coefficients are negative for all displacement distances, indicating that the trailing body will tend towards the wake centerline. In contrast, the pitching moment is seen to decrease slightly with displacement distance and remains negative. In Table 1, $x_{c.p.}/D$ is shown for the various radial displacements. The center of pressure decreases with larger displacements, but is upstream of the center of mass, $x_{c.m.}/D = 1.330$. Both of these conditions (a negative moment and center of pressure upstream of the center of mass) could have an undesirable effect on the trailing body by producing an angle of attack, which in turn could cause a further decrease in the lift coefficient. Ultimately, the trailing body might be completely ejected from the wake core.

Table 1 Center of pressure and static margin for case A with $\Delta x/D = 7.20$

$\Delta r/D$	$x_{c.p.}/D$	$\Delta X_{c.p.} = x_{c.p.}/L - x_{c.m.}/L$
0.05	0.516	−0.326
0.15	0.487	−0.337
0.25	0.276	−0.422

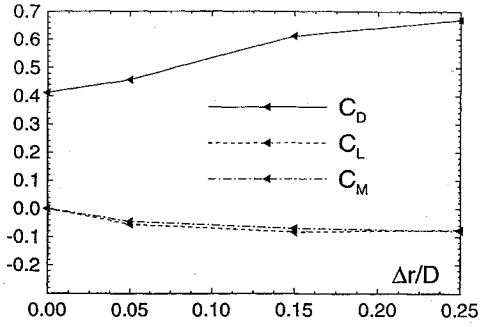

Fig. 14 Force and moment coefficients for case A with $\Delta x/D = 7.20$ at various radial displacements of the trailing body.

Conclusions

A numerical investigation of the flowfield around a blunt body submerged within a supersonic wake was undertaken to determine its aerodynamic characteristics. For coaxial alignments, a toroidal vortex was predicted at the nose of the trailing body. This structure was produced by high pressure near the body shoulder, caused by the impinging shear layer and the low-momentum fluid along the wake centerline. The size and shape of the vortex were highly dependent on the wake profile produced by the leading body. For the sharp leading body (case A), it was found that separation of the two bodies was possible; however, for a blunt leading body (case B), the leading-body drag was much larger than the trailing-body drag, and therefore the two bodies would tend towards each other. This large drag difference suggests that specific forebody geometries may need to be selected to obtain desired separation characteristics.

For increasing radial displacement of the trailing body, the drag coefficient increased with additional exposure to freestream conditions, whereas the predicted negative lift coefficient indicated that the trailing body would tend to move back towards the wake centerline. However, the value of the pitching moment implies that the trailing body would be rotated and produce an angle of attack with the incoming flow. Thus an additional decrease in the lift coefficient would be possible and cause the trailing body to be ejected from the wake.

Acknowledgments

Financial support of the U.S. Army Research, Development and Engineering Center under Contract DAAA21-90-D-0009 is gratefully acknowledged.The authors would like to thank Walter Sturek, Daniel Barnette, and Jubaraj Sahu for their assistance.

References

[1]Hohler, V., and Stilp, A., "Penetration Performance of Segmented Rods at Different Spacing—Comparison with Homogeneous Rods at 2.5–3.5 km/s," *12th International Symposium on Ballistics, Vol. 3* (San Antonio, TX), American Defense Preparedness Association, 1990, pp. 178–187.

[2]Anderson, C. E., Morris, B. L., and Littlefield, D. L., "A Penetration Mechanics Database," Southwest Research Inst., SwRI 3593/001, San Antonio, TX, Jan. 1992.

[3]Roshko, A., and Thomke, G., "Observations of Turbulent Reattachment behind an Axisymmetric Downstream-Facing Step in Supersonic Flow," *AIAA Journal*, Vol. 4, No. 6, 1966, pp. 975–980.

[4]Beheim, M., "Flow in the Base Region of Axisymmetric and Two-Dimensional Configurations," NASA TR R-77, Sept. 1960.

[5]Berner, C., "Aerodynamic Interference Between Projectiles: Measurements and Computation," *14th International Symposium on Ballistics* (Quebec, Canada), American Defense Preparedness Association, 1993, pp. 775–784.

[6]Sahu, J., and Nietubicz, C., "A Computational Study of Cylindrical Segments in the Wake of a Projectile," Ballistic Research Lab., U.S. Army Laboratory Command, BRL-TR-3254, Aberdeen Proving Ground, MD, Aug. 1991; see also Sturek, W., and Nietubicz, C., "Recent Applications of CFD to the Aerodynamics of Army Projectiles at the U.S. Army Ballistic Research Laboratory," AIAA Paper 92-4349, Aug. 1992.

[7]Ober, C. C., "A Computational Study of the Aerodynamics of a Body Immersed in a Compressible Wake," Ph.D. Thesis, Dept. of Mechanical Engineering, Univ. of Texas, Austin, TX, May 1994.

[8]Pulliam, T., and Steger, J., "Implicit Finite-Difference Simulations of Three-Dimensional Compressible Flow," *AIAA Journal*, Vol. 18, No. 2, 1980, pp. 159–167.

[9]Sahu, J., "Numerical Computations of Supersonic Base Flow with Special Emphasis on Turbulence Modeling," *AIAA Journal*, Vol. 32, No. 7, 1994, pp. 1547–1549; also AIAA Paper 92-4352.

[10]Flores, J., "Simulation of Transonic Viscous Wing and Wing–Fuselage Flows Using Zonal Methods," *Proceedings of the First International Symposium on Domain Decomposition Methods for Partial Differential Equations*, edited by R. Glowinski, SIAM, Philadelphia, 1988, pp. 381–415.

[11]Sahu, J., and Steger, J., "Numerical Simulation of Three Dimensional Transonic Flows," AIAA Paper 87-2293, Aug. 1987.

[12]Baldwin, B., and Lomax, H., "Thin Layer Approximation and Algebraic Model for Separated Turbulent Flows," AIAA Paper 78-0257, Jan. 1978.

[13]Deiwert, G., Andrews, A., and Nakahashi, K., "Theoretical Analysis of Aircraft Afterbody Flow," *Journal of Spacecraft and Rockets*, Vol. 24, No. 6, 1987, pp. 496–503.

[14]Danberg, J., and Patel, N., "An Algebraic Turbulence Model for Flow Separation Caused by Forward and Backward Facing Steps," Ballistic Research Lab., U.S. Army Laboratory Command, BRL-MR-3791, Aberdeen Proving Ground, MD, Dec. 1989.

[15]Degani, D., and Steger, J., "Comparison Between Navier–Stokes and Thin-Layer Computations for Separated Supersonic Flow," *AIAA Journal*, Vol. 21, No. 11, 1983, pp. 1604–1606.

[16]Herrin, J., and Dutton, J., "Supersonic Base Flow Experiments in the Near Wake of a Cylindrical Afterbody," *AIAA Journal*, Vol. 32, No. 1, 1994, pp. 77–83.

[17]Nichols, R., Maus, J., Spinetti, R., and Molvik, G., "Calculation of High Speed Base Flows," AIAA Paper 92-2679, July 1992.

[18]Wood, C., "Hypersonic Flow over Spiked Cones," *Journal of Fluid Mechanics*, Vol. 12, April 1962, pp. 614–624.

[19]Ober, C. C., Lamb, J. P., and Kiehne, T. M., "A Computational Study of the Aerodynamics of a Body Immersed in a Supersonic Wake," AIAA Paper 94-3519, Aug. 1994.

[20]Panton, R. L., *Incompressible Flow*, Wiley, New York, 1984.

[21]Lamb, J. P., and Oberkampf, W., "Review and Development of Base Pressure and Base Heating Correlations in Supersonic Flow," *Journal of Spacecraft and Rockets*, Vol. 32, No. 1, pp. 8–23.

Jerry Allen
Associate Editor